FINAL REPORT

A Combined Photo/Electrochemical Reductive Pathway Towards Enhanced PFAS Degradation

SERDP Project ER18-1595

FEBRUARY 2020

David Jassby
The Regents University of California

David Cwiertny
University of Iowa

Bryan Wong
University of California, Riverside

SERDP
DOD ▪ EPA ▪ DOE

Page Intentionally Left Blank

Page Intentionally Left Blank

REPORT DOCUMENTATION PAGE

Form Approved
OMB No. 0704-0188

1. REPORT DATE *(DD-MM-YYYY)*	2. REPORT TYPE	3. DATES COVERED *(From - To)*
02/28/2020	SERDP Final Report	9/12/2018 - 9/12/2020

4. TITLE AND SUBTITLE
A Combined Photo/Electrochemical Reductive Pathway Towards Enhanced PFAS Degradation

5a. CONTRACT NUMBER
18-C-0077

5b. GRANT NUMBER

5c. PROGRAM ELEMENT NUMBER

6. AUTHOR(S)
David Jassby -
The Regents University of California on behalf of its Los Angeles campus
David Cwiertny -
University of Iowa
Bryan Wong -
University of California, Riverside

5d. PROJECT NUMBER
ER18-1595

5e. TASK NUMBER

5f. WORK UNIT NUMBER

7. PERFORMING ORGANIZATION NAME(S) AND ADDRESS(ES)
The Regents of University of California on behalf of its Los Angeles campus
420 Westwood Plaza
5731 Boelter Hall, MC159310
Los Angeles, CA 90095-1593

8. PERFORMING ORGANIZATION REPORT NUMBER
ER18-1595

9. SPONSORING/MONITORING AGENCY NAME(S) AND ADDRESS(ES)
Strategic Environmental Research and Development Program
4800 Mark Center Drive, Suite 17D03
Alexandria, VA 22350-3605

10. SPONSOR/MONITOR'S ACRONYM(S)
SERDP

11. SPONSOR/MONITOR'S REPORT NUMBER(S)
ER18-1595

12. DISTRIBUTION/AVAILABILITY STATEMENT
DISTRIBUTION STATEMENT A. Approved for public release: distribution unlimited.

13. SUPPLEMENTARY NOTES

14. ABSTRACT Perfluoroalkyl substances (PFAS) have been extensively used across multiple industries. Their amphiphilic and inert nature has made them critical components in many commercial and industrial processes. including fire-fighting foams, packaging, and water repellent coatings and materials, and they have subsequently entered the environment through multiple routes: airborne dust, landfill leachate, and industrial and municipal wastewater. The properties that make these compounds attractive, also make them environmentally recalcitrant and mobile. This resistance to degradation arises from the high thermal stability of the carbon-fluoride (C-F) bond, the rigidity of the perfluoroalkyl chain and the lack of reactive substituents in the PFAS molecule. PFAS consist of a long aliphatic hydrophobic tail saturated with F atoms attached to a hydrophilic head group. The elevated stability of the C-F bond arises from the high electronegativity of F which gives this bond a partially ionic character. This bond also becomes shorter and stronger as the number of fluorine atoms on a carbon atom increase. Perfluorooctanoic acid (PFOA) and perfluorooctane sulfonate (PFOS), two members of the PFAS group, have been detected in human serum and milk.

15. SUBJECT TERMS
Photo/Electrochemical Reductive Pathway, Enhanced PFAS Degradation, PFAS

16. SECURITY CLASSIFICATION OF:			17. LIMITATION OF ABSTRACT	18. NUMBER OF PAGES	19a. NAME OF RESPONSIBLE PERSON
a. REPORT	b. ABSTRACT	c. THIS PAGE			David Jassby
					19b. TELEPHONE NUMBER *(Include area code)*
UNCLASS	UNCLASS	UNCLASS	UNCLASS	29	919-357-4992

Page Intentionally Left Blank

FINAL REPORT

Project: ER18-1595

TABLE OF CONTENTS

Page

LIST OF FIGURES

Page

LIST OF TABLES

Page

ACRONYMS AND ABBREVIATIONS

BDE — Bond dissociation energy
BZT — Benzethonium chloride, a cationic surfactant
cDCE — Cis - dichloroethylene
CNT — Carbon nanotube
CPS — Counts per second
CTAB — Cetrimonium bromide, a cationic surfactant
DDBS — Dodecylbenzenesulfonate , an anionic surfactant
DFT — Density functional theory
DO — Dissolved oxygen
EPA — Environmental Protection Agency
ET — Electron Transfer
IC — Ion chromatography
LCMS — Liquid chromatography – mass spectroscopy
PCM — Polarizable continuum model
PFAS — Perfluoroalkyl substances
PFBS — Perfluorobutanesulfonic acid
PFCA — Perfluoroalkyl carboxylates
PFHpA — Perfluoroheptanoic acid
PFHxS — Perfluorohexane sulfonate
PFNA — Perfluorononanoic acid
PFOA — Perfluorooctanoic acid
PFOS — Perfluorooctane sulfonate
PFSA — Perfluoroalkyl sulfonates
TB — Tert-butanol
TCE —Trichloroethylene
TDTAB — Tetradecyl trimethyl bromide, a cationic surfactant
TX — Triton X-100
UV — Ultraviolet
XPS — X-ray photoelectron spectroscopy

Introduction

Perfluoroalkyl substances (PFAS) have been extensively used across multiple industries[1]. Their amphiphilic and inert nature has made them critical components in many commercial and industrial processes. including fire-fighting foams, packaging, and water repellent coatings and materials[2], and they have subsequently entered the environment through multiple routes: airborne dust,[3] landfill leachate,[4] and industrial and municipal wastewater[5]. The properties that make these compounds attractive, also make them environmentally recalcitrant and mobile[6]. This resistance to degradation arises from the high thermal stability of the carbon-fluoride (C-F) bond, the rigidity of the perfluoroalkyl chain and the lack of reactive substituents in the PFAS molecule[7]. PFAS consist of a long aliphatic hydrophobic tail saturated with F atoms attached to a hydrophilic head group. The elevated stability of the C-F bond arises from the high electronegativity of F which gives this bond a partially ionic character[8,9]. This bond also becomes shorter and stronger as the number of fluorine atoms on a carbon atom increase. Perfluorooctanoic acid (PFOA) and perfluorooctane sulfonate (PFOS), two members of the PFAS group, have been detected in human serum and milk[10]. They have been demonstrated to be human carcinogens, as well as having adverse effects on the immune system.[11]. The most likely exposure route for humans is through drinking water and the EPA has established a health advisory of 70 ng/L of PFOS and PFOA[12]. The standard methods used to treat PFAS contaminated water are adsorption with activated carbon, ion exchange resins and separation using nanofiltration or reverse osmosis membranes[13,14]. However, these methods do not degrade the chemicals, and subsequent treatment is required[13,15,16].

Two main PFAS groups are perfluoroalkyl carboxylates (PFCA), which have a carboxyl group as the hydrophilic head and perfluoroalkyl sulfonates (PFSA) having a sulfonate group as the head. The hydrophobic tail in both of these compounds is a long aliphatic chain where all the hydrogen atoms are replaced by fluorine (F). While chemical oxidation has been fairly successful in the breakdown of PFCAs, PFSAs have been particularly challenging to degrade[17]. In fact, chemical oxidation methods, including hydroxyl radicals, are not effective at degrading these compounds, making them particularly challenging to remove. The elevated stability of PFOS stems from its weak polarization, thermal stability (i.e., C_2H_5–H of 101 kcal/mol vs. C_2F_5–F of 127 kcal/mol, and CF_3–CF_3 of 99 kcal/mol vs. CH_3–CH_3 of 89 kcal/mol) and oxidative resistance (i.e., $F + e^- \rightarrow F^-$, $E^0 = 3.6$ V).[8,9,17] To date, very few methods have been identified that can destroy this molecule; these methods include electrooxidation at high current densities (for C-F bond cleavage, 9 V at a distance of 0.5 cm to 16.6 V at a distance of 2 cm at constant current density)[18] using specialized electrodes (e.g. boron-doped diamond)[19], incineration,[20] sonolysis,[4] and reduction via hydrated electrons[21,22].

UV-based degradation methods are widely used to destroy organic contaminants in water.[25] However, the destruction of PFOS by UV alone (with low- or medium- pressure mercury lamps) at room temperature is very slow (10 days, 48% defluorination with initial 40 uM PFOS under N_2 atmosphere).[26] The mechanism responsible for PFOS degradation under UV irradiation is believed to involve the generation of hydrated electrons (h_e), which are produced from the ionization of water by sufficiently energetic photons (with a wavelength below 185 nm) (Equation 1).[27] The high reduction potential of h_e allows them to reduce the C-F bond ($E^{\theta}_{e} = -2.87$ V; $E^{\theta}_{C\text{-}F} \leq -2.7$ V).[17] However, the high reactivity of the h_e (coupled to the low number of sufficiently energetic photon generated from standard medium pressure UV lamps) leads to many competing side reactions (e.g., Equations 2 and 3), which rapidly consume them and lead to the slow defluorination rates observed in pure UV systems.[17,28] In fact, studies have indicated that the lifetime of h_e in solution is approximately 10^{-7} sec, with a diffusion pathway estimated to be <2 nm long.[17,28] Thus, strategies to increase the effectiveness of h_e include the elimination of competing side reactions, increasing the number of h_e generated, and increasing the probability of reaction between h_e and the target molecule. Increasing the h_e yield has been demonstrated by adding compounds such as sulfite[22]

and iodide[8], while competing reactions can be eliminated through the addition of hydroxyl-radical scavangers (e.g., tert-butanol), increasing pH, or eliminating dissolved O_2 .[27,29] However, the addition of chemicals to water, which, depending on the water's final intended use, usually requires further treatment to remove these impurities.[30]

$$2H_2O + h\nu \rightarrow \cdot OH + H_3O^+ + h_e \quad (1)$$
$$\cdot OH + h_e \rightarrow OH^- \qquad k=3.0\times10^{10}\ M^{-1}s^{-1} \quad (2)$$
$$H^+ + h_e \rightarrow \cdot H + H_2O \quad k=2.3\times10^{10}\ M^{-1}s^{-1} \quad (3)$$

To the best of our knowledge, strategies to increase the reaction rate of hydrated electrons with target molecules (without changing environmental conditions, such as temperature), have not been explored. Developing such strategies could enable the effective degradation of recalcitrant compounds without the need for chemical additives or energy intensive degradation processes. One such strategy involves the lowering of the activation energy of the C-F bond. While there have been reports on catalytic processes capable of facilitating the defluorination of aromatic fluorinated compounds, no such catalysts have been identified for aliphatic species. An alternative method to lower the activation energy of these bonds involves the "priming" of target molecules through direct electron transfer (ET); in this method, an electron is forced onto the target molecule, without leading to the dissociation of any chemical bonds. [31]·[41]. The driving force for this ET can be provided through a potential difference between the surface of a cathode and a sorbed target molecule (such as PFOS), with greater differences driving faster ET rates.[31,32] If the potential difference is large enough, and there is sufficient energy in the system, the receiving entity can dissociate, leading to bond cleavage.[32] However, if there is insufficient energy in the system, the electron can return to the donating entity (i.e., the system relaxes).[31,33] When the electron transfers to the "receiving" entity, the entity becomes excited and forms a transient radical anion; in this excited state, chemical bonds in the receiving entity destabilize due to a perturbation of the entity's electron cloud.[33,34] Thus, in this excited state, the molecules are more susceptible to external energy input that can lead to bond dissociation.[33] ET between molecules sorbed onto a conductive surface can be initiated through the application of an electrical potential to this surface.[35] In an aqueous environment, if this potential exceeds the over-potential associated with water electrolysis, gas evolution and energy consumption increase. However, below this threshold, ET occurs without any water splitting, making the process energy-efficient.

Here, we examine how potential-induced ET processes can dramatically increase the defluorination rate of PFOS molecules by UV-generated h_e in an additive-free system. Importantly, the ET reaction is performed at potentials below water electrolysis, which dramatically reduces energy consumption in the system. The defluorination reactions are explored under different electrode surface chemistries, aqueous constituents, and applied potentials. The degradation products and defluorination rates are characterized by liquid chromatography – mass spectroscopy (LCMS), ion selective electrodes, and ion chromatography (IC). In addition, density functional theory (DFT) is used to explore the impact of electron addition to the PFOS molecule in terms of bond lengths and the C-F bond activation energy. Our results demonstrate how the specific adsorption of PFOS onto electrodes with tailored chemical properties can facilitate ET between the electrode and the adsorbed PFOS, which enables UV-generated h_e to rapidly defluorinate PFOS. To the best of our knowledge, this is the first study to demonstrate the coupling of electrochemically-induced ET to photo-assisted degradation reactions, which dramatically increases the degradation rate of aqueous recalcitrant organic contaminants. We also extend this study to investigate the effect of the head group (carboxyl vs sulfonate) and alkyl chain length on the extent of PFAS degradation, and on other co-contaminants including chlorinated solvents such as trichloroethylene and cis-dichloroethylene which are found in groundwater along with PFAS.

1. Results

1.1. Impact of different CNT surfactant stabilizers, potential, solution pH and electrode surface area on defluorination of PFOS

While UV-generated h_e alone are able to defluorinate PFOS, the defluorination rate is very slow, with only 0.012 ppm (0.63 μM) F^- (0.4% defluorination) generated after 2 hours of exposure (control experiment

in Figure 1a). To test the UV-electrochemical system, we used a Pt-coated titanium (Ti) plate and a graphite sheet as cathodes (with a Pt-coated Ti plate as anode), and found that the defluorination rate showed no clear improvement after applying 2 V (Figure 2). Since CNTs are excellent current collectors, as well as capable of sorbing contaminants (though not capable of producing h_e by any recognized mechanism), we used percolating networks of CNTs, deposited on a polymeric support, and functionalized them with different surfactants as sorption sites/electrodes with the goal of facilitating ET between the current collector and sorbed contaminants[36–38]. Here, surfactants with different structure and functional groups were used to stabilize aqueous suspensions of CNTs, which were subsequently deposited on the support; the hydrophobic tail of the surfactant tethers these molecules to the CNT backbone through hydrophobic interactions, with the charged hydrophilic head capable of potentially functioning as ion exchange sites for the target molecules[39]. These electrodes (Figure 3, with CNT layer thickness 6 μm) were immersed in a PFOS solution and a -0.58 V *vs.* Ag/AgCl (2 V cell potential) was applied to the CNT electrode (functioning as a cathode against a Pt-coated Ti anode). A marked increase in F^- concentration was observed when the cationic surfactant CTAB was used as the CNT stabilizer [F^- of 0.21 ppm (11.05 μM) after 2 hours, or 7.33% defluorination at a defluorination rate of 0.10 ppm/h (5.26 μM/h)] (Figure 1a). Similarly, when the cationic surfactants TDTAB and BZT were used to stabilize the CNTs, enhanced defluorination was observed, but to a lesser extent [F^- of 0.11 ppm (5.79 μM) and 0.13 ppm (6.84 μM) after 2 hours, representing 3.67% and 4.33% defluorination, respectively] (Figure 1a). However, CNTs stabilized with the anionic surfactant DDBS or the non-ionic surfactant Triton X-100 did not show any accelerated defluorination (Figure 1a).

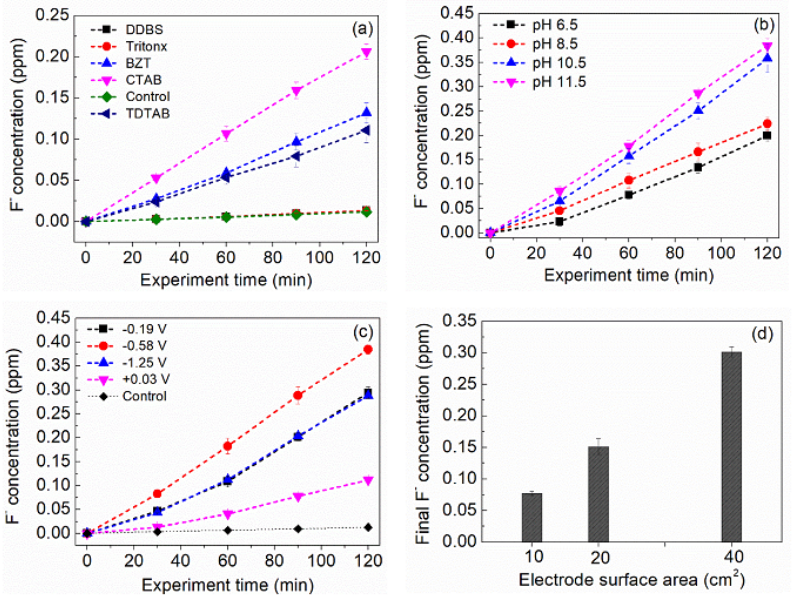

Figure 1. (a) Impact of different CNT surfactant stabilizers on defluorination of PFOS (UV + -0.58 V *vs*. Ag/AgCl at pH 6.5 with 50 cm^2 electrode surface area; Control = no electrode); (b) impact of initial pH on defluorination (CNT/CTAB cathode with 50 cm^2 electrode surface area, -0.58 V *vs.* Ag/AgCl, UV); (c) impact of applied potential on PFOS defluorination (CNT/CTAB cathode with 50 cm^2 electrode surface area, UV, pH 11.5; Control = no electrode); (d) impact of CNT/CTAB cathode surface area on PFOS defluorination (UV, -0.58 V *vs*. Ag/AgCl, pH 11.5).

Protons are effective scavengers of h_e (Equation 3)[17,28]. Thus, it is expected that a drop in proton concentrations will reduce competition for h_e, increasing their availability to react with the sorbed PFOS on the cathode. We investigated the impact of initial solution pH on PFOS degradation on a CNT/CTAB cathode with -0.58 V vs. Ag/AgCl applied to its surface (Figure 1b). As expected, increasing the pH of the solution from 6.5 to 11.5 increased the final F^- concentration from 0.21 ppm to 0.38 ppm (Figure 1b), and

the defluorination rate rose from 0.10 ppm/h (5.26 μM/h) to 0.19 ppm/h (10.27 μM/h). Even though the change in proton concentrations explored in these experiments was exponential, the increase in defluorination rate was not. Thus, while the solution pH is important, it is not the governing factor in determining defluorination rates.

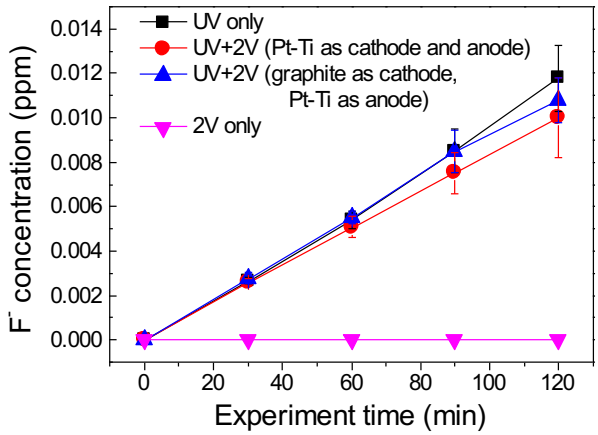

Figure 2. Defluorination performance under different reaction conditions

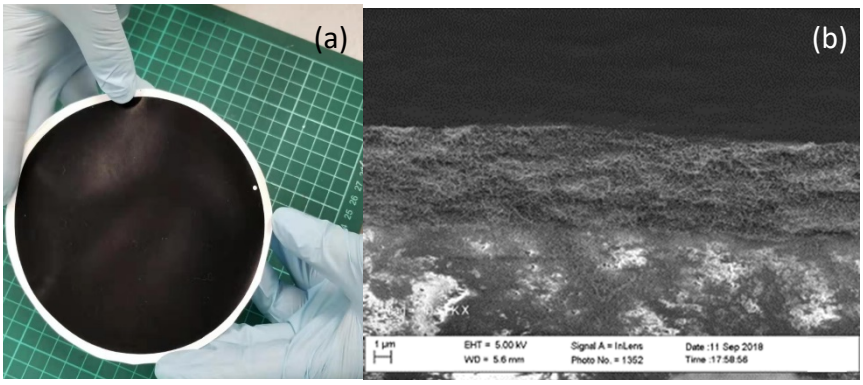

Figure 3. (a) CNT/CTAB electrode; (b) scanning electron microscope image of CNT/CTAB electrode surface

The impact of the applied potential on PFOS defluorination rates using CTAB-functionalized CNT electrodes was also investigated (Figure 1c). By applying 0 V, 1 V, 2 V, and 3 V cell potentials (with CNT electrode as cathode), the relative potential (*vs.* Ag/AgCl) of the CNT/CTAB electrode was +0.03 V, -0.19 V, -0.58 V, and -1.25 V. The current density under these conditions was 0.0166 μA/cm^2, 0.0038 ± 0.0002 mA/cm^2, 0.056 ± 0.002 mA/cm^2 and 0.1152 ± 0.004 mA/cm^2, respectively. At cell potential ≥ -0.58 V vs. Ag/AgCl, increasing the cell potential (and current density) enhanced the defluorination rate from 0.15 ppm/h (7.83 μM/h) to 0.19 ppm/h (10.27 μM/h). Critically, at 0 V (i.e., CNT/CTAB electrode immersed in the solution with no external potential applied), the CNT/CTAB had a potential of +0.03 V *vs.* Ag/AgCl, and we observed an increased defluorination rate from 0.006 ppm/h (0.30 μM/h) (the control with no electrode present) to 0.057 ppm/h (3.02 μM/h). However, when -1.25 V *vs.* Ag/AgCl (3 V cell potential) were applied to the CNT/CTAB electrode, the defluorination rate declined from 0.19 ppm/h (10.27 μM/h) to 0.15 ppm/h (7.75 μM/h) while the final F^- concentrations declined from 0.39 ppm (20.52 μM) to 0.29 ppm (15.26 μM) (Figure 1c). Cyclic voltammetry (CV) measurements using the CNT/CTAB as a working electrode showed that the onset of electrolysis occurs at -0.30 V *vs*. an Ag/AgCl reference (Figure 4). At -

1.25 V *vs*. Ag/AgCl (3 V cell potential), water electrolysis was occurring, which competed with PFOS for electrons. Also, we cannot rule out electrostatic repulsion between the negatively charged PFOS and CNT/CTAB cathode surface since the final F^- concentration after a 2 hour reaction declined from 0.087 ppm (4.58 μM) (CNT/CTAB surface not connected to a counter Pt-Ti counter electrode, UV, pH 6.5) to 0.076 ppm (4.00 μM) when the CNT/CTAB electrode was used as an anode (cell potential of 2 V, UV, pH 6.5) (Figure 5). Thus, both the cathodic potential on the CNT/CTAB electrode and the sorption of PFOS on the surface of the electrode are necessary to increase PFOS susceptibility to the h_e attack, which increases the overall defluorination rate.

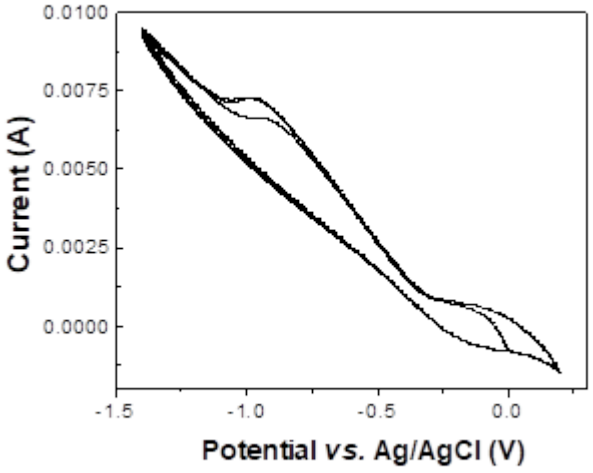

Figure 4. Cyclic voltammetry curve with CNT/CTAB, Pt-Ti plate and Ag/AgCl as working, counter, and reference electrodes

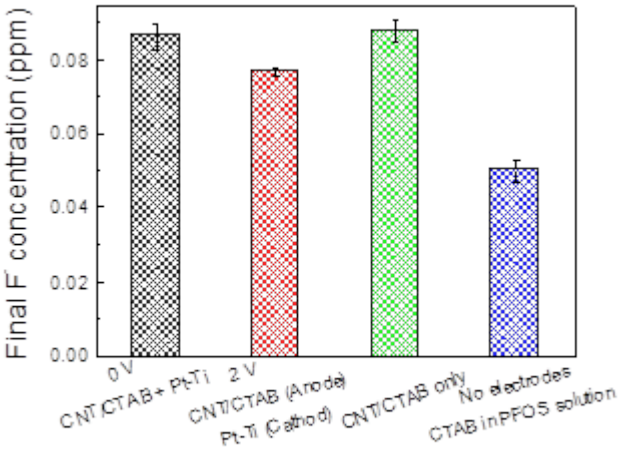

Figure 5. Defluorination performance in UV reaction systems with/without CNT/CTAB electrode under oxic condition after 2-hour reaction with initial pH = 6.5

To determine whether the PFOS defluorination reaction is indeed a surface reaction taking place on the CNT/CTAB electrode, we varied the surface area of the electrode immersed into the PFOS solution (10, 20, and 40 cm^2) (Figure 1d). After 2 hours reaction (UV, -0.58 V *vs*. Ag/AgCl), the final F^- concentration was 0.08 ppm (4.21 μM), 0.15 ppm (7.89 μM), and 0.30 ppm (15.79 μM), for the 10, 20, and 40 cm^2 electrode, respectively, with concentrations doubling with each doubling of surface area.

1.2. **PFOS adsorption on electrode surface**

X-ray photoelectron spectroscopy (XPS) was employed to evaluate the adsorption of PFOS on the cathode surface. Full spectrum XPS scans (of gently rinsed and air-dried electrode surfaces) clearly showed the presence of a fluoride peak on the CNT/CTAB electrode after it was immersed in the PFOS solution for 30 minutes, with 4.45% of the atomic mass on the surface attributable to fluoride (Figure 6 a). Since no other fluoride containing species were in the solution, this is a strong indication that PFOS successfully sorbed to the CNT/CTAB material. Moreover, F signal was also detected after PFOS adsorption test with a cell potential of 2 V (CNT/CTAB-1, in Figure6 a), implying that potential did not stop PFOS adsorption. While no fluoride signal was detected on the full XPS spectra obtained from the CNT/TDTAB and CNT/BZT surfaces (Figure 6 a), a high-resolution scan of the F 1s region did detect some fluoride on these surfaces, although peak intensity was low (Figure 6 b). When the CNT/DDBS and CNT/TritonX surfaces were examined with the full scan (Figure 6 a) and the high-resolution F 1s scan (Figure 6 c), no fluoride was detected, suggesting that PFOS adsorption did not occur on these two types of cathodes. Furthermore, on the CNT/CTAB electrode surface, the high-resolution F 1s XPS spectra (Figure 6 d) showed that the peak shifted from 689.2 ± 0.2 eV to 688.2 ± 0.2 eV after 2 hours reaction (UV, -0.58 V *vs*. Ag/AgCl, pH 6.5), consistent with -CF_2-CF_2- bonds being partially reduced to CF_2-CHF-/-CF_2-CH_2-/CHF-CH_2- bonds[40]. These XPS results suggest that PFOS adsorption is an essential step for ET enhancement of the defluorination process, and, that PFOS reduction occurs on the cathode surface (driven by interactions with h_e).

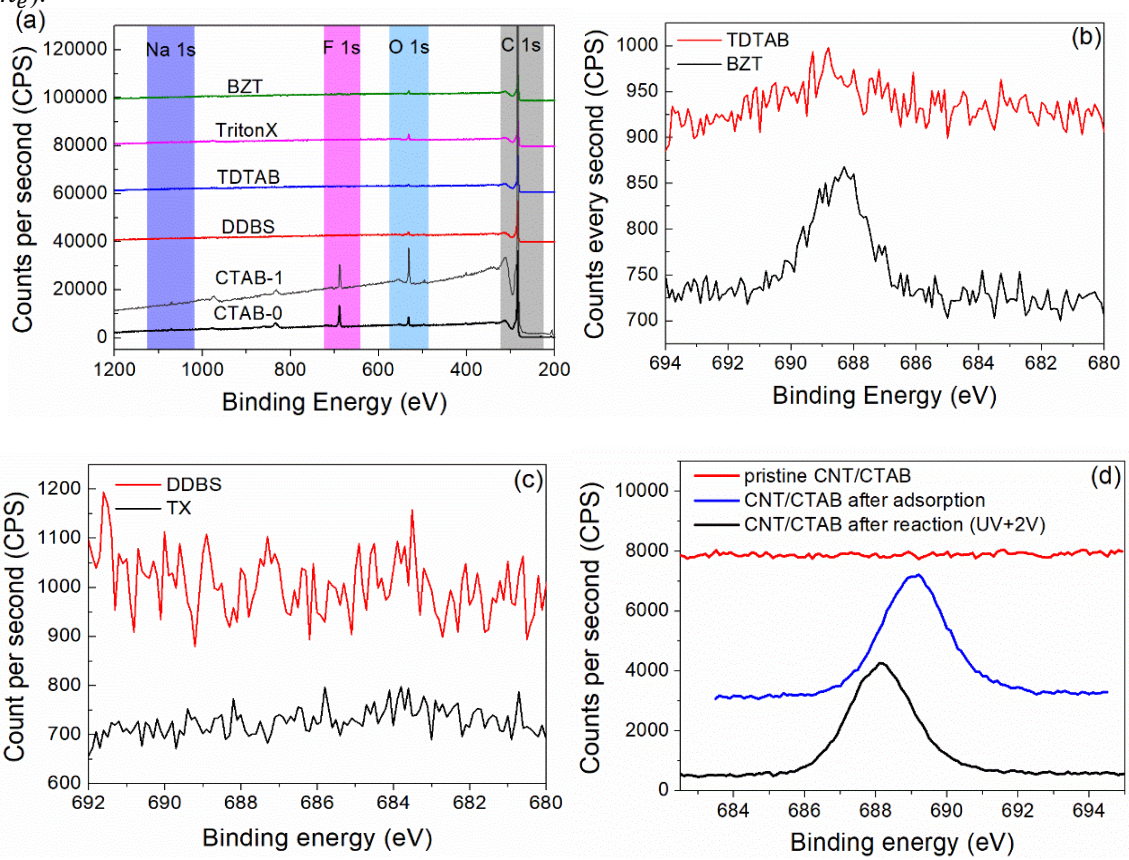

Figure 6. (a) Full XPS spectra of CNT/DDBS, CNT/BZT, CNT/TritonX, CNT/TDTAB, and CNT/CTAB(-0) electrodes after PFOS adsorption at pH 6.5 for 30 min (CNT/CTAB-1, after PFOS adsorption at pH 6.5 with a cell potential of 2 V for 30 min); (b) high-resolution F 1s XPS spectra of cationic CNT/BZT and CNT/TDTAB electrodes after PFOS adsorption test; (c) high-resolution F 1s XPS spectra of CNT/DDBS and CNT/TX electrodes after PFOS adsorption test; (d) high-resolution F 1s XPS spectra of pristine CNT/CTAB electrode and electrodes before and after PFOS degradation (UV, -0.58 V *vs*. Ag/AgCl, pH 6.5).

1.3. Defluorination driven by hydrated electrons

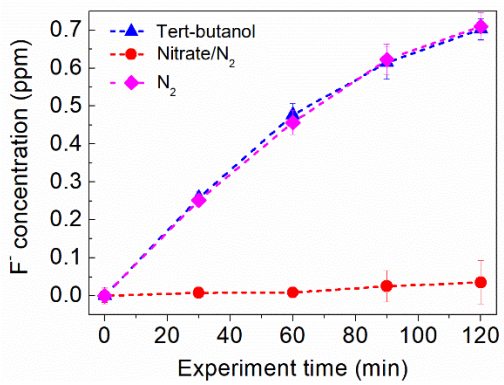

Figure 7. PFOS defluorination in the presence of TB, nitrate, or N_2 (UV, -0.58 V *vs*. Ag/AgCl, pH 11.5)

To explore the role of h_e in PFOS defluorination reactions, we carried out defluorination experiments (CNT/CTAB cathode, UV, -0.58 V *vs*. Ag/AgCl, pH 11.5) with different solution additives (Figure 7). Nitrate is an effective h_e scavenger (Equation 4)[41]; when 15 mM of nitrate were added, very little fluoride was liberated, which confirms the importance of h_e to the defluorination process. Dissolved oxygen (DO) acts as a highly effective h_e scavenger (Equations 5 and 6)[28]. By continuously purging N_2 through the system, DO concentrations were reduced to below 0.1 ppm; once the experiment commenced, defluorination was greatly enhanced , with a final F^- concentration (after 2 hours) of 0.71 ppm (37.37 μM), a nearly two-fold increase over concentrations measured under oxygenated conditions (Figure 7 vs. Figure 1b), with defluorination rates greatly enhanced to 0.46 ppm/h (24.03 μM F^-/h, a 2.34-fold increase over oxygenated conditions). Hydroxyl radicals formed during the UV-induced h_e generation process (Equation 1) can scavenge h_e, and since both of these species are co-located during generation, hydroxyl radicals act as potent scavengers. When we added 15 mM of tert-butanol, a known hydroxyl radical scavenger, to the solution, the defluorination rate increased to 0.48 ppm/h (25.08 μM F^-/h) (83 times higher than that in the UV-only system), a result very similar to the N_2 purging (Figure 7). Together, these results demonstrate the critical part that h_e play in PFOS defluorination.

$$h_e + NO_3^- \rightarrow (\cdot NO_3)^{2-} \quad k=1.0\times10^{10}\ M^{-1}s^{-1} \quad (4)$$

$$h_e + O_2 \rightarrow \cdot O_2^- \quad k=1.9\times10^{10}\ M^{-1}s^{-1} \quad (5)$$

$$h_e + \cdot O_2^- \rightarrow O_2^{2-} \quad k=1.3\times10^{10}\ M^{-1}s^{-1} \quad (6)$$

1.4. PFOS removal, desulfonation, and defluorination

In addition to fluoride, sulfate and PFOS concentrations were measured at the end of the 2-hour experimental period. The reaction of h_e and PFOS can lead to the cleavage of the sulfonate group from the PFOS molecule, which transforms to sulfate in water[26,29]. In general, PFOS removal (defined as the final PFOS concentration divided by the initial PFOS concentration) was greater than desulfonation (defined as the final sulfate concentration divided by the total theoretical sulfate concentration generated after 100% PFOS degradation); desulfonation was nearly always greater than defluorination (defined as the final fluoride concentration divided by the total theoretical fluoride concentration generated after 100% PFOS degradation), except when tert-butanol (the hydroxyl radical scavenger) was added to the solution (Table 1). When a PFOS solution (pH 11.5) was exposed to medium-pressure UV light, no PFOS or sulfate were removed, and the % defluorination was extremely low (0.4± 0.10%). When a CNT/CTAB/Pt-Ti electrode pair was added to the solution (0 V), desulfonation, and defluorination increased to 57.1 ± 6.2%, and 3.7 ± 0.1%, respectively (Table 1). Upon purging with N_2, PFOS removal, desulfonation, and defluorination increased to 81.0 ± 3.1%, 70.0 ± 3.4% and 6.8 ± 1.0%. When a potential was applied to the electrode pair (-0.58 V vs. Ag/AgCl), these ratios further increased to 86.2 ± 5.9%, 77.8 ± 4.5% and 23.7 ± 1.2%. Interestingly, the addition of tert-butanol did not change defluorination (23.3 ± 0.9%), but desulfonation dropped dramatically (to 24.1 ± 2.2%). At a moderate pH (8.5), desulfonation and defluorination were somewhat lower than at higher pH. Based on the data presented in Table 1, it can be

deduced that anaerobic conditions, high pH, and moderate potentials are favorable for both defluorination and desulfonation of PFOS.

Table 1. PFOS removal and degradation performance after 2 hours of reactions under different conditions.

Experiment conditions	PFOS removal (%)	Desulfonation (%)	Defluorination (%)	Defluorination rate[a] (ppm/h; μM F^-/h)
$UV^{w/t}$, pH 11.5	/	-	0.4 ± 0.1	0.0057; 0.30
UV/0 V, pH 11.5	NM	57.1 ± 6.2	3.7 ± 0.1	0.05738; 3.02
UV/0 V, N_2, pH 11.5	81.0 ± 3.1	70.0 ± 3.4	6.8 ± 1.0	0.13794; 7.26
UV/2 V, pH 8.5	NM	49.4 ± 9.0	7.5 ± 0.1	0.11362; 5.98
UV/2 V, pH 11.5	NM	73.2 ± 11.2	12.8 ± 0.2	0.19513; 10.27
UV/2 V, N_2, pH 11.5	86.2 ± 5.9	77.8 ± 4.5	23.7 ± 1.2	0.45657; 24.03*
UV/1 V, pH 11.5	NM	47.4 ± 5.6	9.8 ± 0.1	0.14877; 7.83
UV/3 V, pH 11.5	NM	57.6 ± 6.7	9.6 ± 0.4	0.14725; 7.75
UV/2 V, TB, pH 11.5	65.6 ± 7.1	24.1 ± 2.2	23.3 ±0.9	0.47652; 25.08*

Note: /, no removal within 2 h; -, sulfate concentration after 2h was below the detection limit; $^{w/t}$, no CNT/CTAB electrode in reaction system; TB, tert-butanol; [a], linear fitting with r^2 >0.98; *, data within first hour was used for calculation to minimize impact of mass-transport limitations; NM, not measured.

1.5 PFOS degradation pathway and products

Analysis of the products generated from PFOS decay were explored using LCMS for the UV/2V system under N_2 gas at pH 11.5 (from Table 1, PFOS removal of ~86%, desulfonation of ~78% and defluorination of ~24%). Degradates from other photoelectrochemical systems from Table 1 were not explored.

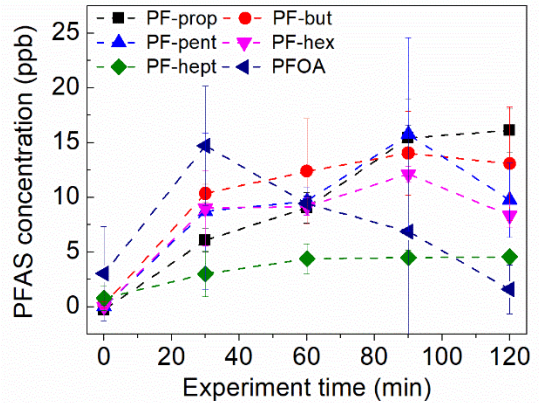

Figure 8. Evolution of PFOS degradation products over time.

PFOS decay occurred concomitantly with the formation of PFOA and several shorter chain perfluorinated acids (Figure 8), the formation of which was confirmed using commercially available standards. PFOA concentration was greatest at our earliest sampling point but steadily degraded over the remainder of the reaction time. At all sampling points, the least abundant degradate was perfluoroheptanoic acid. Perfluorohexanoic and pentanoic acid species accumulated over the first 90 minutes, but their concentrations decreased in the final sampling point. The concentration of shorter chain length perfluorobutyric acid and pentafluoropropionic acid increased monotonically over time, and were present at the greatest abundance at the final sampling point after 2 hours.

The amount of products detected and quantified is far below the initial concentration of PFOS used in these experiments. To assess potential non-reactive mass losses in our electrode systems, we also conducted

control studies in the absence of UV light and applied potential to measure the uptake of PFOS on CTAB functionalized electrode materials. These sorption studies, which were conducted at an identical electrode loading (based on surface area ~0.067 cm^2/mL) to that used in photoelectrochemical systems, revealed some uptake capacity for the electrode materials (2.6 μg PFOS/cm^2 of electrode area). In contrast, DDBS functionalized electrodes did not exhibit any detectable uptake.

We note that no attempts were made to evaluate the relative degree to which degradates sorbed to the electrode surface, such that dissolved concentrations reported in Figure 8 may not reflect the total mass of each species generated from PFOS degradation (i.e., some degradates may remain surface associated). We also did not attempt to identify, via non-target analysis, any previously unidentified PFAS degradates that may have been generated photoelectrochemically under these conditions, which may also explain the difference observed between initial PFOS mass and measured degradate mass.

1.6 Modeling the impact of electron addition to PFOS

To explore the impact of ET on the various PFOS bonds, we performed density functional theory (DFT) calculations. To simplify the calculations, we focused only on the impact of additional electrons to PFOS, and neglected other (potentially important) interactions, such as between CTAB and PFOS and CNTs and PFOS. Both the geometries of the native (-1 charge) and excess-charged (-2 charge) PFOS systems were optimized in the presence of a conductor-like polarizable continuum model (PCM) by Tomasi and co-workers[42–46], which creates a solute cavity via a set of overlapping spheres to calculate the solvent reaction field. A detailed description of the computational approach can be found in the SI. For the native system, we obtained strong bond dissociation free energies of ~102 kcal/mol (on average), which reflect the strength of the polar C–F bond (Figure 9). Upon the addition of a single electron to the PFOS molecule (which formed the excess-charged state), we obtained C-F bond dissociation free energies of ~30 kcal/mol (Figure 9), which are significantly reduced compared to its native configuration.

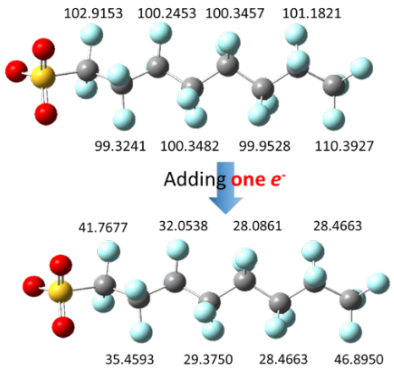

Figure 9. Change of bond dissociation free energy after adding one electron onto native PFOS molecule.

In addition to changes in C-F bonds, we used DFT to explore the bond length of the C-S bond in response to ET (Figure 10). Similar to the C-F bonds, the C-S bond weakens as electrons are added to PFOS. Interestingly, the C-S bond length (a proxy to bond strength, with longer distances pointing towards lower strength[47]) responds rather weakly to the first ET event (increasing from 1.92 $\dot{A}$ to 1.94 $\dot{A}$. However, the addition of a second electron more than doubles the bond length (to 4.22 $\dot{A}$), which strongly suggests bond dissociation.

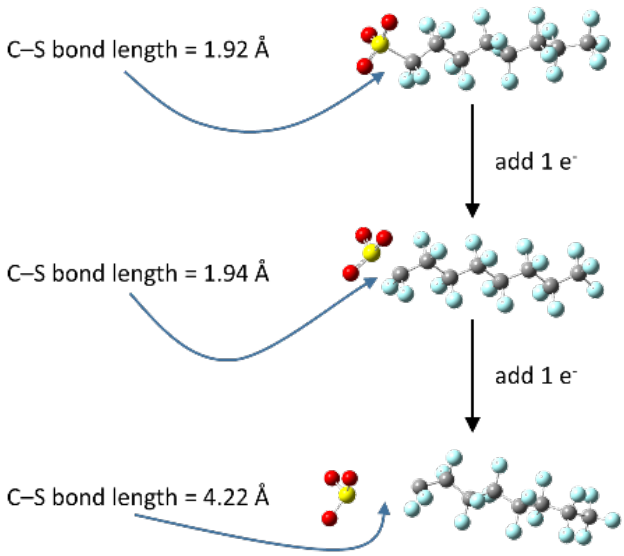

Figure 10. Change of C-S bond length after adding one or two consecutive electrons onto PFOS molecule

1.7 Effect of chain length and headgroup on degradation rate

Table 2: Surface coverage on the electrode (measured by XPS)

Species	Fluoride surface coverage
PFNA	0.16%
PFOA	0.17%
PFHpA	below detection limit
PFOS	4.45%
PFHxS	0.65%
PFBS	below detection limit

In this section, we report on the degradation rates of PFCA and PFSA molecules with different chain lengths. The PFCA molecules we tested were PFHpA (7 carbons), PFOA (8 carbons), and PFNA (9 carbons), while the PFSA molecules were PFBS (4 carbons), PFHxS (6 carbons), and PFOS (8 carbons) (Figure 11). For PFHpA (7 carbon), the F concentration was 0.64 ± 0.03 ppm after 2 hours with UV-only. Under UV/0V conditions, the fluoride concentrations increased to 0.7 ± 0.11 ppm (a 9.3% increase), although this increase was not statistically significant (p=0.29 by unpaired t-test). However, when a potential of 2 V was applied, there was a significant increase to 0.76 ±0.05 ppm (an 18.75% increase over UV-only conditions). For PFOA (8 carbon), degradation under UV-only conditions resulted in a fluoride concentration of 0.69 ± 0.06 ppm after two hours, which increased to 0.79 ± 0.07 ppm (14.5% increase) under UV/0V conditions, although this increase was not statistically significant. The application of 2 V further increased the rate of defluorination, with a final F concentration of 0.98 ± 0.17 ppm (a 42% increase over UV-only conditions); this increase was statistically significant. In PFNA (9-carbon) degradation, the final fluoride concentration was 0.67 ± 0.03 ppm under UV-only conditions, which increased marginally to 0.68 ± 0.03 under 0 V conditions (not significant). However, under UV/2V conditions, the final fluoride concentration increased significantly to 1.12 ± 0.12 ppm (a 67% increase over UV-only conditions). Based on these results, under UV-only conditions, the PFCA chain length had little impact on the defluorination rate when only hydrated electrons were involved (0.64 ppm, 0.69 ppm and 0.67 ppm for 7, 8 and 9 carbon chain compounds, respectively). This data matches previous studies where defluorination rates by hydrated electrons were

found to be independent of chain length[9]. Immersing the electrodes (UV/0V conditions) resulted in a small increase in defluorination rates of PFHpA and PFOA (9.3% and 14.5% respectively), and only a marginal increase in the defluorination of PFNA. However, the increased defluorination was not statistically significant, and it is unclear why an uncharged electrode surface would contribute to increased defluorination.

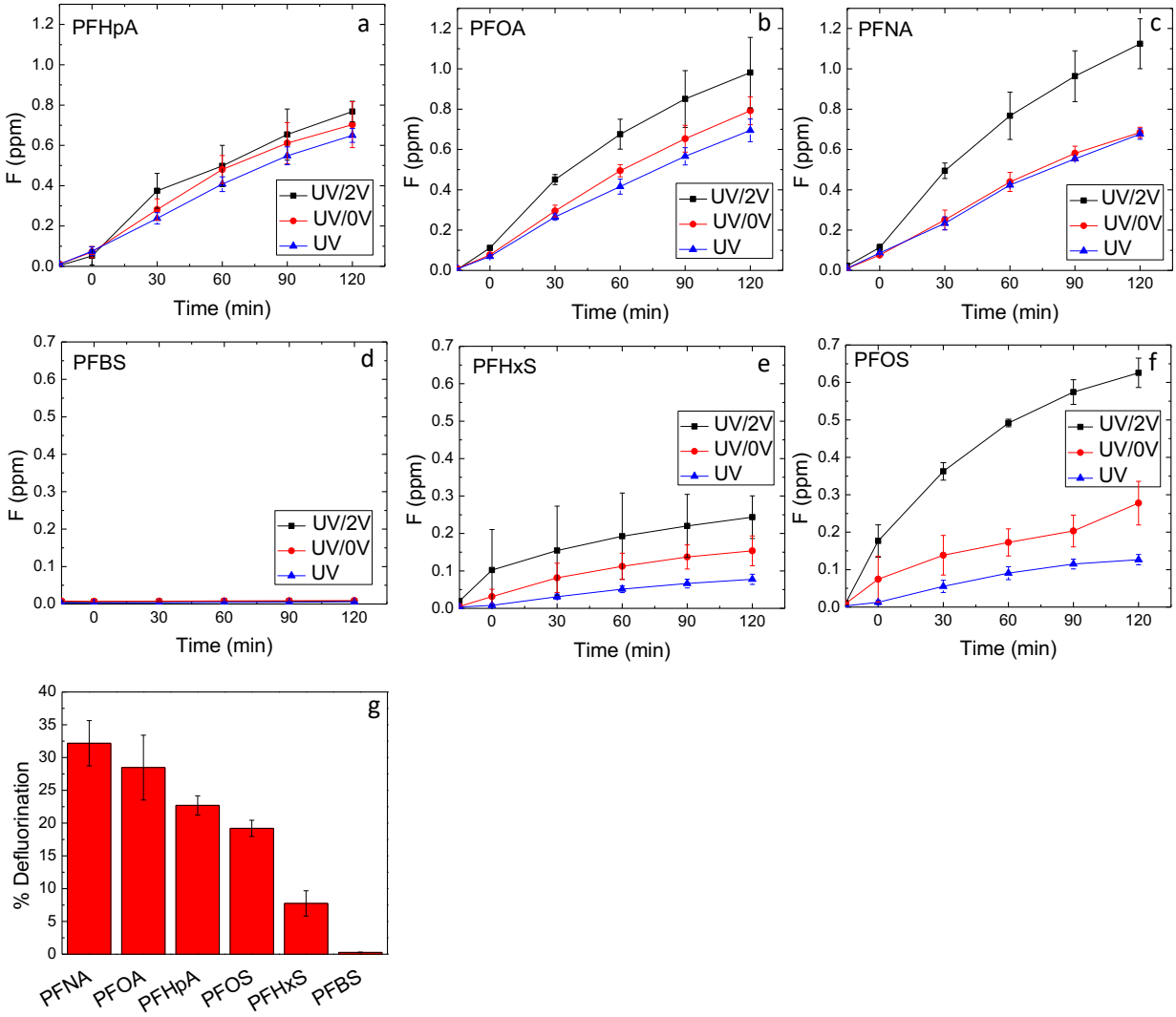

Figure 11: Defluorination of PFSAs with different chain lengths under UV/2V, UV/0V and UV-only (i.e., no electrode was present) conditions: (a) PFHpA, (b) PFOA, (c) PFNA, (d) PFBS, (e) PFHxS and (f) PFOS at pH 11.5 and N_2 purging. The UV/0V conditions imply that the electrodes were immersed in the solution, but no external potential was applied, while UV implies that no electrodes were present; and (g) % Defluorination of six PFAS compounds under UV/2V conditions

Under UV/2V conditions, there was a small increase in the defluorination rate of PFHpA (8.5% increase in the final F concentration over UV/0V conditions). We observed a greater enhancement in defluorination for PFOA (24% increase in F concentration over UV/0V), and an even greater increase during PFNA degradation (67% increase in F concentration over UV/0V). In order to determine whether this increase can

be attributed to potential-driven ET between the electrode and the sorbed molecules, we performed XPS measurements (Table 2) to quantify the amount of PFCA sorbed on the electrode surface, which is the first step in the ET process. A previous study on the sorption of PFCAs on activated carbon showed that longer chain compounds exhibited higher sorption, which is associated with the more hydrophobic nature of the longer perfluorinated tail[24]. This would indicate that PFNA should have the highest sorption, followed by PFOA and then PFHpA. However, our results did not agree with this. While no fluoride could be detected on the surface of the electrode tested for sorption of PFHpA, the electrodes tested with PFNA and PFOA showed some fluoride surface coverage (0.16% and 0.17% respectively). However, this sorbed fluoride is not significant and it is unlikely that any surface reaction is causing enhanced defluorination. Since the data clearly demonstrates that the longer-chained molecules exhibit better defluorination under these conditions, and since there is no significant difference in sorption of PFOA and PFNA on the electrode surface, this enhanced defluorination rate for longer chained compounds is not caused by sorption of PFCAs on to the electrode. Previous studies used density function theory (DFT) to calculate the effect of the chain length on the bond dissociation energy (BDE) of the C-F bond in PFAS molecules. They found that the BDE for C-F bonds associated with longer chain compounds are lower. The average BDE for PFNA is 108.6 kcal/mol, while that for PFOA is 108.8 kcal/mol. The BDE for PFHpA is quite a bit higher, at 109.4 kcal/mol, which makes it harder for the C-F bond in PFHpA to break. Hence, we speculate that the reason for higher defluorination rate of longer chained PFCAs is due to the reduced BDE of their C-F bonds.

The defluorination of PFSA molecules with different chain lengths (PFBS (4 carbons), PFHxS (6 carbons), and PFOS (8 carbons)) was studied under UV, UV/0V and UV/2V conditions (Fig. 2d, e, f). For PFBS, very little defluorination was observed under all three conditions (0.006 ± 0.001 ppm with UV, 0.009 ± 0.002 ppm with UV/0V, and 0.008 ± 0.001 ppm with UV/2V) (Figure 11d). When studying the 6-carbon PFHxS, the fluoride concentrations under UV-only conditions reached a very low 0.07 ± 0.01 ppm. Immersing electrodes in the solution enhanced degradation rate by 100% to 0.15 ± 0.03 ppm, and the application of 2 V enhanced the defluorination further, increasing fluoride concentrations from 0.15 ± 0.03 ppm to 0.24 ± 0.06 ppm (a 60% increase) after 2 hours of reaction (Figure 11e). For 8-carbon PFOS, the fluoride concentration under UV conditions was 0.12 ± 0.01 ppm, increasing by 125% to 0.27 ± 0.05 ppm when electrodes were immersed into the solution (Figure 11f). The application of 2 V further increased the defluorination rate, resulting in a final fluoride concentration of 0.63 ± 0.03 ppm (a 133% increase). While we observed some (albeit, very limited) breakdown of 6 carbon compound PFHxS (0.07 ± 0.01 ppm) and 8 carbon compound PFOS (0.12 ± 0.01 ppm) under UV-only conditions, no PFBS (4 carbon compound) breakdown (0.006 ± 0.001 ppm) was observed. This agrees with previous studies showing that shorter chain PFSAs are much harder to break down by hydrated electrons[48]. While immersing the electrode and applying potential did not impact the PFBS degradation rate, results were different in the case of the two longer chained compounds. For PFHxS and PFOS, simply immersing the electrode increased defluorination rate significantly, whereas the application of 2 V enhanced it even further. Several studies on the sorption of different chain-length sulfonated PFAS molecules have shown that longer chain PFAS are sorbed on to granular activated carbon to a much greater extent[49]. To test the sorption of PFAS on the CNT electrode, we performed XPS, with the results shown in Table 2. The data in Table 2 shows that, as expected, the carbon chain length had a big impact on PFSA adsorption. As in the case of PFCAs, the enhanced defluorination observed when the 2 V potential was applied is likely due to potential- driven ET between the electrode and the sorbed molecule, followed by an attack by a hydrated electron. Since sorption on the electrode surface is the first step in the defluorination process, and is critical for the ET between the electrode and target molecule to occur, it follows that shorter chain compounds which are sorbed to a lesser extent will exhibit lower defluorination rates. It is possible that the enhanced defluorination of PFHxS and PFOS that we observed in the absence of an applied cell potential can be attributed to ET caused by the open circuit potential (-0.03 V), which possibly causes bond destabilization to a lesser extent, making the C-F bonds more susceptible to breakdown by hydrated electrons.

The % defluorination (Figure 11g) was calculated as the concentration of fluoride measured in the sample at the end of two hours, expressed as a percent of the fluoride concentration expected on 100% defluorination. The highest defluorination was observed for 9-carbon PFNA, at 32 ± 3.4% defluorination. For the slightly shorter 8-carbon PFOA, the defluorination was 28.5 ± 5%. For 7-carbon chained compound PFHpA, the defluorination further dropped to 22.7 ± 1.5%. For sulfonated compounds, the 8-carbon chain

PFOS reached 19.2 ± 1.2% defluorination. For the 6-carbon chained PFHxS, the final defluorination was 7.8 ± 1.9%. However, the 4-carbon PFBS experienced barely any defluorination (0.3 ± 0.03%). These values are in line with our hypothesis that sulfonated PFASs are harder to defluorinate than carboxylated PFAS, and in compounds with the same headgroup, the ease of defluorination decreases with decrease in chain length.

1.8 Degrading PFAS mixtures

To test the effect of mixtures on PFAS defluorination rates, experiments were carried out with 5 ppm of each of the PFAS molecules tested previously along with 50mM of NaClO4 (Figure 12). Under UV/0V conditions, the final F concentration resulting from the defluorination of the PFAS mixture was 2.8 ± 0.3 ppm (Figure 12a). When 2 V potential was applied, the fluoride concentration increased by 16.1% to 3.2 ± 0.1 ppm (Figure 12a). Figures 12b and 12c show a comparison between the F concentrations observed during degradation of the mixture and the expected F concentration based on adding F concentrations observed at the end of two hours during degradation of the individual compounds. Under UV/0V conditions, the experimental values (2.8 ± 0.3 ppm) are close to the expected values from defluorination of individual compounds (2.6 ± 0.3 ppm), a 7.1% difference albeit not a statistically significant one. However, under UV/2V conditions, significant differences emerge. Specifically, the experimentally observed fluoride concentration resulting from degrading the PFAS mixture was 3.2 ± 0.1 ppm, significantly lower than the expected values from the degradation of individual compounds (3.8 ± 0.4 ppm), a 18.8% difference. Studies on the sorption of PFCAs on bamboo activated carbon and IRA67 resin showed a significant reduction in adsorption when a mixture of PFCA was tested[50][51]. This was due to the PFCA molecules competing for adsorption sites. Thus, we speculate that competition between PFSA molecules for adsorption sites on the CNT electrode limits ET and reduces overall PFAS degradation rates.

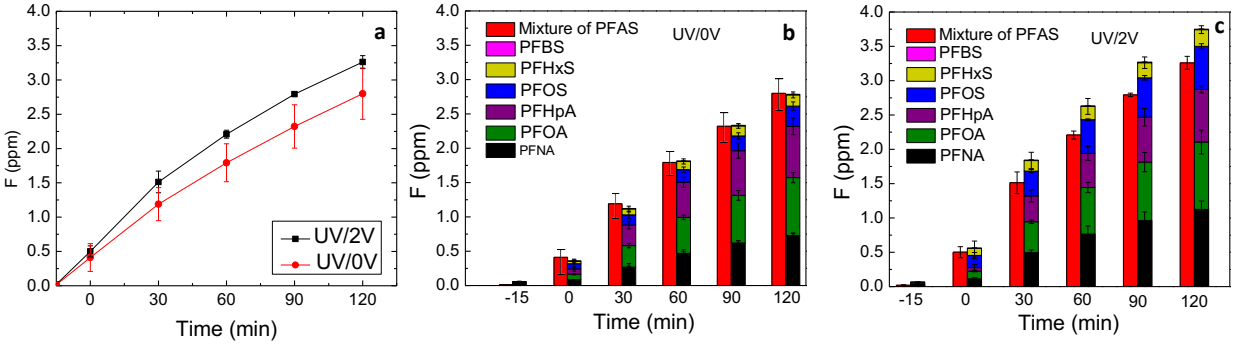

Figure 12: Defluorination rates of mixture of PFAS (a) Comparison with and without applied potential, and comparison between experimentally observed defluorination of mixture and expected defluorination based on individual compounds tested under conditions of (b) UV/0V and (c) UV/2V

1.9 Probing the mechanism of PFOS defluorination

ET reactions occur when an electron is passed from the electrode surface to the molecule, typically when these two entities are in close proximity. The driving force for this reaction is a potential difference between the electrode and the molecule[19]. If the potential difference is large enough, thus leading to a sufficiently

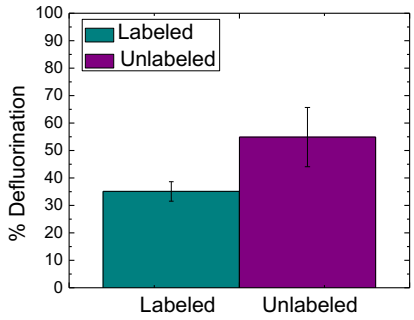

Figure 13: Percent defluorination for Labeled (C^{13}) and non-labeled (C^{12}) PFOS under UV/2V (pH 11.5, bubbled with N_2 gas).

energetic electron, this electron transfer reaction can lead to bond cleavage[52]. However, if the potential difference is insufficient, the electron can relax and return to the electrode. When the electron is transferred to the PFOS molecule, the molecule shifts to an excited state and a radical anion is formed. In this excited state, molecular bonds are weakened (i.e., elongated) and are more susceptible to cleavage by an external hydrated electron[53]. The strength of a covalent bond is a function of the atomic species that compose the bond, as well as their atomic weight[54]. Specifically, heavier atoms form stronger bonds[55][56]. Therefore, when comparing the defluorination of PFOS molecules sorbed onto a CNT electrode, we hypothesize that PFOS molecules containing heavier atoms (i.e., isotopically labeled PFOS) will undergo slower defluorination rates because their C-F bonds will not become as "perturbed" as a result of ET compared to unlabeled PFOS. This is known as the kinetic isotope effect, wherein heavier isotopes of PFOS will have a lower vibrational frequency, making it harder to break the bonds. In general, it is easier to break bonds with C^{12} than with C^{13}. The electron added through externally applied potential will have a greater effect in weakening the C^{12}-F bond compared to the C^{13}-F bond, resulting in lower defluorination of the isotopically labelled PFOS[57,58]. Results in Figure 13 show that the defluorination rate of isotopically labeled PFOS (C^{13}) was lower than the non-labeled (C^{12}) PFOS (35% for isotopically labelled PFOS vs. 52% for non labelled PFOS). This confirms that the defluorination occurs due to C-F bond excitation by the ET step and subsequent breakdown by the hydrated electron.

1.10 Degradation of chlorinated solvents

The degradation rates of trichloroethylene (TCE) and cis-dichloroethylene (cDCE) were measured using the same experimental conditions used to assess PFAS defluorination. For TCE (Figure 14a), the final Cl concentration under UV-only conditions was 1.53 ± 0.13 ppm, increasing marginally to 1.62 ± 0.36 ppm under conditions of UV/0V. Under UV/2V conditions, the final Cl concentration was 1.58 ± 0.3 ppm at the end of two hours. There was a sudden jump in Cl concentration in the last 30 minutes under UV/2V conditions. The reason for this is unclear. However, the error bars for all these conditions were overlapping, indicating that there was no significant difference in chloride evolution rates. For cDCE (Figure 14b), the Cl concentration after two hours was 1.42 ± 0.08 ppm under UV only conditions. Under UV/0V conditions,

final Cl concentration was 1.6 ± 0.4 ppm, and the degradation rate under UV/2V conditions was the lowest, with a final Cl concentration of 1.15 ± 0.04 ppm. However, it can be seen that the Cl concentrations are very close until the 90-minute sample was collected, and then deviated significantly in the final 30 minutes (Figure 14b). The reason for this is unclear, although error bars for UV/0V and UV are quite large, making this difference statistically insignificant. These results indicate that the immersion of electrodes and application of potential likely did not impact degradation rates of chlorinated solvents.

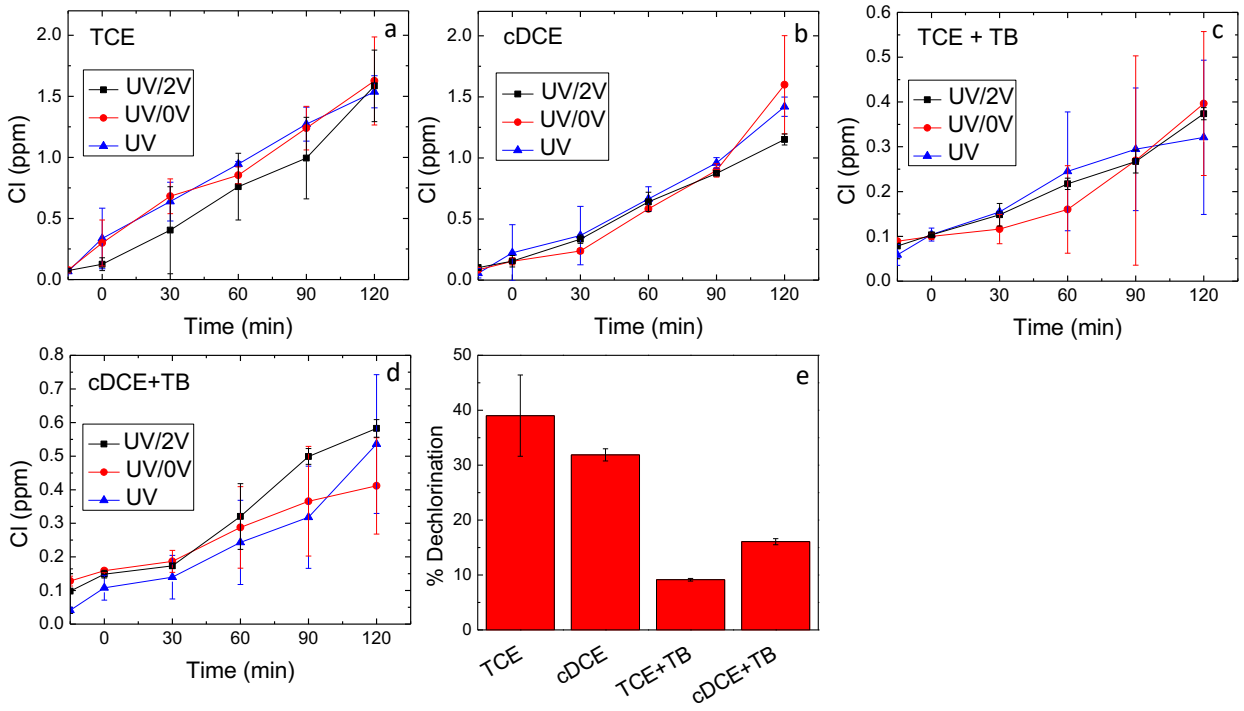

Figure 14: Degradation of (a) TCE and (b) cDCE under UV/2V, UV/0V and UV only; and (e) % dechlorination of TCE and cDCE in the absence and presence of t-butanol

Degradation of aqueous TCE and cDCE has been shown to be carried out by direct UV photolysis, generally in the presence of chlorine or H_2O_2[59][60]. Such advanced oxidation processes work by generating hydroxyl radicals that break down TCE and cDCE. Medium pressure UV light (with no additional chemical additives) has also been shown to generate OH radicals when water is irradiated with it [61]. Hence, it is possible that the degradation of TCE and cDCE observed in Figures 14a and b was due to oxidation by hydroxyl radicals rather than reduction by hydrated electrons. To test whether oxidation was indeed the dominant mechanism, we added 15 µM of TB, a hydroxyl radical scavenger, to the solution. Results are shown in Figures 14c and d. The addition of TB is expected to quench hydroxyl radicals, and reduce the possibility of direct oxidation. As can be seen, the rate of chloride evolution fell dramatically, with a final chloride concentration between 0.3-0.4 ppm for TCE and 0.4-0.6 ppm for cDCE (compared to 1.58 ± 0.3 ppm and 1.15 ± 0.04 ppm in the absence of TB, a 75% and 48% decrease for TCE and cDCE, respectively). Again, no significant difference was observed between the different operating conditions (UV-only, UV/0 V, and UV/2V) ((Figure 14c and 14d). Therefore, it is reasonable to conclude that in these experiments, both TCE and cDCE were primarily degraded through an oxidative reaction with hydroxyl radicals. While chloride evolution was suppressed in the presence of TB, it did not go to zero, suggesting that hydrated electrons possibly play in the dechlorination of these compounds, albeit a relatively minor one compared to hydroxyl radicals.

For enhanced reductive dechlorination from potential-driven ET to occur, sorption of the molecule on to the electrode is a prerequisite. To test whether this is taking place, we performed XPS analysis of the electrode material immersed in solutions of TCE and cDCE (data not shown). However, no chlorine could be detected on the electrode surface. indicating that no sorption occurred. Therefore, in order the promote

degradation by this pathway, electrode materials that are more capable of sorbing chlorinated solvents need to be fabricated.

Economic analysis of the process

We estimated the cost of our process using PFOS as target pollutant, and compared our cost to that of other techniques. Based on our bench-scale process, under optimal operating conditions (anoxic conditions, pH 11.5), the process consumes 0.033 kWh/μmol F^- from PFOS: with 0.031 kWh consumed by the medium pressure UV lamp, and 0.002 kWh consumed by electrochemical process. This energy consumption is 1/8th of the energy input consumed by the UV-only system under similar conditions (0.264 kWh/μmol F^-). Since PFOS contamination is often associated with groundwater, which tends to have low dissolved O_2 concentrations, it is unlikely that degassing will be necessary. Thus, the overall operational cost of our process is \$0.11842/mg F^- (\$0.00225/μmol F^-), assuming an electricity cost of \$0.07/kWh (typical cost for industrial power in USA). Comparisons of this cost to existing UV-based treatment methods is complicated by the fact that these treatments, while often exhibiting higher defluorination rates, require the addition of chemicals to the water, which (depending on the final fate of this water) may require further treatment before disposal (e.g., reverse osmosis to remove residual sulfite or sulfate). Comparison to other PFOS degradation methods, such as direct electrooxidation at high potentials, sonolysis, or thermal degradation, is complicated by the different operating conditions (e.g., different initial PFOS concentrations), as well as that some (particularly older) studies do not report on defluorination rates.

References

[1] Z. Wang, J.C. DeWitt, C.P. Higgins, I.T. Cousins, A never-ending story of per-and polyfluoroalkyl substances (PFASs)?, (2017).

[2] X. Dauchy, V. Boiteux, C. Bach, C. Rosin, J.-F. Munoz, Per-and polyfluoroalkyl substances in firefighting foam concentrates and water samples collected near sites impacted by the use of these foams, Chemosphere. 183 (2017) 53–61.

[3] K. Harada, S. Nakanishi, N. Saito, T. Tsutsui, A. Koizumi, Airborne Perfluorooctanoate May Be a Substantial Source Contamination in Kyoto Area, Japan, Bull. Environ. Contam. Toxicol. 74 (2005) 64–69. https://doi.org/10.1007/s00128-004-0548-0.

[4] J. Cheng, C.D. Vecitis, H. Park, B.T. Mader, M.R. Hoffmann, J.I.E. Cheng, C.D. Vecitis, Sonochemical Degradation of Perfluorooctane Sulfonate (PFOS) and Perfluorooctanoate (PFOA) in Landfill Groundwater : Environmental Matrix Effects Sonochemical Degradation of Perfluorooctane Sulfonate (PFOS) and Perfluorooctanoate (PFOA) in Landfil, Environ. Sci. Technol. 42 (2008) 8057–8063. https://doi.org/10.1021/es8013858.

[5] M. Trojanowicz, A. Bojanowska-Czajka, I. Bartosiewicz, K. Kulisa, Advanced Oxidation/Reduction Processes treatment for aqueous perfluorooctanoate (PFOA) and perfluorooctanesulfonate (PFOS) – A review of recent advances, Chem. Eng. J. 336 (2018) 170–199. https://doi.org/10.1016/j.cej.2017.10.153.

[6] K.A. Barzen-Hanson, S.C. Roberts, S. Choyke, K. Oetjen, A. McAlees, N. Riddell, R. McCrindle, P.L. Ferguson, C.P. Higgins, J.A. Field, Discovery of 40 classes of per-and polyfluoroalkyl substances in historical aqueous film-forming foams (AFFFs) and AFFF-impacted groundwater, Environ. Sci. Technol. 51 (2017) 2047–2057.

[7] V. Ochoa-Herrera, J.A. Field, A. Luna-Velasco, R. Sierra-Alvarez, Microbial toxicity and biodegradability of perfluorooctane sulfonate (PFOS) and shorter chain perfluoroalkyl and polyfluoroalkyl substances (PFASs), Environ. Sci. Process. Impacts. 18 (2016) 1236–1246.

[8] H. Park, C.D. Vecitis, J. Cheng, N.F. Dalleska, B.T. Mader, M.R. Hoffmann, Reductive degradation of perfluoroalkyl compounds with aquated electrons generated from iodide photolysis at 254 nm, Photochem. Photobiol. Sci. 10 (2011) 1945–1953. https://doi.org/10.1039/c1pp05270e.

[9] H. Park, C.D. Vecitis, J. Cheng, W. Choi, B.T. Mader, M.R. Hoffmann, Reductive defluorination of aqueous perfluorinated alkyl surfactants: Effects of ionic headgroup and chain length, J. Phys. Chem. A. 113 (2009) 690–696. https://doi.org/10.1021/jp807116q.

[10] W. Völkel, O. Genzel-Boroviczény, H. Demmelmair, C. Gebauer, B. Koletzko, D. Twardella, U. Raab, H. Fromme, Perfluorooctane sulphonate (PFOS) and perfluorooctanoic acid (PFOA) in human breast milk: results of a pilot study, Int. J. Hyg. Environ. Health. 211 (2008) 440–446.

[11] European Food Safety Authority., Opinion of the Scientific Panel on Contaminants in the Food chain on Perfluorooctane sulfonate (PFOS), perfluorooctanoic acid (PFOA) and their salts, EFSA J. 653 (2008) 1–131.

https://doi.org/10.2903/j.efsa.2008.653.
[12] EPA, Drinking water health advisories for PFOA and PFOS, (2016).
[13] C.Y. Tang, Q.S. Fu, A.P. Robertson, C.S. Criddle, J.O. Leckie, Use of reverse osmosis membranes to remove perfluorooctane sulfonate (PFOS) from semiconductor wastewater, Environ. Sci. Technol. 40 (2006) 7343–7349.
[14] K.E. Carter, J. Farrell, Removal of perfluorooctane and perfluorobutane sulfonate from water via carbon adsorption and ion exchange, Sep. Sci. Technol. 45 (2010) 762–767.
[15] V. Ochoa-Herrera, R. Sierra-Alvarez, Removal of perfluorinated surfactants by sorption onto granular activated carbon, zeolite and sludge, Chemosphere. 72 (2008) 1588–1593. https://doi.org/10.1016/j.chemosphere.2008.04.029.
[16] I. Ross, J. McDonough, J. Miles, P. Storch, P. Thelakkat Kochunarayanan, E. Kalve, J. Hurst, S. S. Dasgupta, J. Burdick, A review of emerging technologies for remediation of PFASs, Remediation. 28 (2018) 101–126. https://doi.org/10.1002/rem.21553.
[17] C.D. Vecitis, H. Park, J. Cheng, B.T. Mader, M.R. Hoffmann, Treatment technologies for aqueous perfluorooctanesulfonate (PFOS) and perfluorooctanoate (PFOA), Front. Environ. Sci. Eng. China. 3 (2009) 129–151. https://doi.org/DOI 10.1007/s11783-009-0022-7.
[18] H. Lin, J. Niu, S. Ding, L. Zhang, Electrochemical degradation of perfluorooctanoic acid (PFOA) by Ti/SnO2–Sb, Ti/SnO2–Sb/PbO2 and Ti/SnO2–Sb/MnO2 anodes, Water Res. 46 (2012) 2281–2289. https://doi.org/10.1016/j.watres.2012.01.053.
[19] K.E. Carter, J. Farrell, Oxidative destruction of perfluorooctane sulfonate using boron-doped diamond film electrodes, Environ. Sci. Technol. (2008). https://doi.org/10.1021/es703273s.
[20] P.H. Taylor, T. Yamada, R.C. Striebich, J.L. Graham, R.J. Giraud, Investigation of waste incineration of fluorotelomer-based polymers as a potential source of PFOA in the environment, Chemosphere. 110 (2014) 17–22. https://doi.org/10.1016/j.chemosphere.2014.02.037.
[21] H. Tian, J. Gao, H. Li, S.A. Boyd, C. Gu, Complete Defluorination of Perfluorinated Compounds by Hydrated Electrons Generated from 3-Indole-acetic-acid in Organomodified Montmorillonite, Sci. Rep. 6 (2016) 1–9. https://doi.org/10.1038/srep32949.
[22] Y. Gu, W. Dong, C. Luo, T. Liu, Efficient Reductive Decomposition of Perfluorooctanesulfonate in a High Photon Flux UV/Sulfite System, Environ. Sci. Technol. 50 (2016) 10554–10561. https://doi.org/10.1021/acs.est.6b03261.
[23] C.Y. Tang, Q.S. Fu, C.S. Criddle, J.O. Leckie, Effect of flux (transmembrane pressure) and membrane properties on fouling and rejection of reverse osmosis and nanofiltration membranes treating perfluorooctane sulfonate containing wastewater, Environ. Sci. Technol. 41 (2007) 2008–2014. https://doi.org/10.1021/es062052f.
[24] Y. Zhi, J. Liu, B. Sun, J. Ma, D.L. Sedlak, V. Ochoa-Herrera, R. Sierra-Alvarez, R. Mailler, J. Gasperi, Y. Coquet, A. Buleté, E. Vulliet, S. Deshayes, S. Zedek, C. Mirande-Bret, V. Eudes, A. Bressy, E. Caupos, R. Moilleron, G. Chebbo, V. Rocher, C.J.A.F. Kwadijk, I. Velzeboer, A.A. Koelmans, M.C. Hansen, M.H. Børresen, M. Schlabach, G. Cornelissen, A. Schaefer, C.P. Higgins, R.G. Luthy, K.U. Goss, G. Bronner, T. Harner, M. Hertel, T.C. Schmidt, Calgon Carbon, T.D. Appleman, E.R. V Dickenson, C. Bellona, C.P. Higgins, S.T.M.L.D. Senevirathna, S. Tanaka, S. Fujii, C. Kunacheva, H. Harada, B.R. Shivakoti, R. Okamoto, Nanofiltration and granular activated carbon treatment of perfluoroalkyl acids, Environ. Sci. Technol. 40 (2016) 7108–7109. https://doi.org/10.1021/es060004p.
[25] J.M. Herrmann, Heterogeneous photocatalysis: Fundamentals and applications to the removal of various types of aqueous pollutants, Catal. Today. 53 (1999) 115–129. https://doi.org/10.1016/S0920-5861(99)00107-8.
[26] Y. Shibata, Photodegradation of PerfluorooctaneSulfonate by UV Irradiation in Water and Alkaline 2-Propanol, Environ. Sci. Technol. 41 (2007) 5660–5665.
[27] X.J. Lyu, W.W. Li, P.K.S. Lam, H.Q. Yu, Insights into perfluorooctane sulfonate photodegradation in a catalyst-free aqueous solution, Sci. Rep. 5 (2015) 1–6. https://doi.org/10.1038/srep09353.
[28] G. V. Buxton, C.L. Greenstock, W.P. Helman, A.B. Ross, Critical Review of rate constants for reactions of hydrated electrons, hydrogen atoms and hydroxyl radicals (·OH/·O−in Aqueous Solution, J. Phys. Chem. Ref. Data. 17 (1988) 513–886. https://doi.org/10.1063/1.555805.
[29] L. Jin, P. Zhang, Photochemical decomposition of perfluorooctane sulfonate (PFOS) in an anoxic alkaline solution by 185nm vacuum ultraviolet, Chem. Eng. J. 280 (2015) 241–247. https://doi.org/10.1016/j.cej.2015.06.022.
[30] F. Edition, W.H.O. (Who), Guidelines for Drinking-water Quality, World Health. (2011). https://doi.org/10.1016/S1462-0758(00)00006-6.
[31] R.A. Marcus, On the Theory of Electron-Transfer Reactions. VI. Unified Treatment for Homogeneous and Electrode Reactions, J. Chem. Phys. 43 (1965) 679–701. https://doi.org/10.1063/1.1696792.

[32] F. Maran, M.S. Workentin, Dissociative Electron Transfer, Electrochem. Soc. Interface. 11 (2002) 44–49.
[33] P. Christopher, H. Xin, S. Linic, Visible-light-enhanced catalytic oxidation reactions on plasmonic silver nanostructures, Nat. Chem. 3 (2011) 467–472. https://doi.org/10.1038/nchem.1032.
[34] G.L. Closs, L.T. Calcaterra, N.J. Green, K.W. Penfield, J.R. Miller, Distance, stereoelectronic effects, and the Marcus inverted region in intramolecular electron transfer in organic radical anions, J. Phys. Chem. 90 (1986) 3673–3683. https://doi.org/10.1021/j100407a039.
[35] P. Chen, R.L. McCreery, Control of Electron Transfer Kinetics at Glassy Carbon Electrodes by Specific Surface Modification, Anal. Chem. 68 (1996) 3958–3965. https://doi.org/10.1021/ac960492r.
[36] L. Tang, A. Iddya, X. Zhu, A. V. Dudchenko, W. Duan, C. Turchi, J. Vanneste, T.Y. Cath, D. Jassby, Enhanced Flux and Electrochemical Cleaning of Silicate Scaling on Carbon Nanotube-Coated Membrane Distillation Membranes Treating Geothermal Brines, ACS Appl. Mater. Interfaces. 9 (2017) 38594–38605. https://doi.org/10.1021/acsami.7b12615.
[37] W. Duan, G. Chen, C. Chen, R. Sanghvi, A. Iddya, S. Walker, H. Liu, A. Ronen, D. Jassby, Electrochemical removal of hexavalent chromium using electrically conducting carbon nanotube/polymer composite ultrafiltration membranes, J. Memb. Sci. 531 (2017) 160–171. https://doi.org/10.1016/j.memsci.2017.02.050.
[38] A. V. Dudchenko, C. Chen, A. Cardenas, J. Rolf, D. Jassby, Frequency-dependent stability of CNT Joule heaters in ionizable media and desalination processes, Nat. Nanotechnol. 12 (2017) 557–563. https://doi.org/10.1038/nnano.2017.102.
[39] L. Vaisman, H.D. Wagner, G. Marom, The role of surfactants in dispersion of carbon nanotubes, Adv. Colloid Interface Sci. 128–130 (2006) 37–46. https://doi.org/10.1016/j.cis.2006.11.007.
[40] G. Nansé, E. Papirer, P. Fioux, F. Moguet, A. Tressaud, Fluorination of carbon blacks: An X-ray photoelectron spectroscopy study: I. A literature review of XPS studies of fluorinated carbons. XPS investigation of some reference compounds, Carbon N. Y. 35 (1997) 175–194. https://doi.org/10.1016/S0008-6223(96)00095-4.
[41] M.C. Gonzalez, A.M. Braun, VUV photolysis of aqueous solutions of nitrate and nitrite, Res. Chem. Intermed. 21 (1995) 837–859. https://doi.org/10.1163/156856795X00512.
[42] M.A. Aguilar, F.J.O. del Valle, J. Tomasi, Electron correlation and solvation effects. II. The description of the vibrational properties of a water molecule in a dielectric given by the application of the polarizable continuum model with inclusion of correlation effects, Chem. Phys. 150 (1991) 151–161. https://doi.org/10.1016/0301-0104(91)80125-2.
[43] F.J.O. del Valle, J. Tomasi, Electron correlation and solvation effects. I. Basic formulation and preliminary attempt to include the electron correlation in the quantum mechanical polarizable continuum model so as to study solvation phenomena, Chem. Phys. 150 (1991) 139–150. https://doi.org/10.1016/0301-0104(91)80124-Z.
[44] F.J.O. Del Valle, R. Bonaccorsi, R. Cammi, J. Tomasi, Electron correlation and solvation effects. Part 3. Influence of the basis set and the chemical composition on the solvation energy components evaluated with the quantum mechanical polarizable continuum model, J. Mol. Struct. THEOCHEM. 230 (1991) 295–312. https://doi.org/10.1016/0166-1280(91)85186-B.
[45] J. Tomasi, R. Bonaccorsi, R. Cammi, F.J.O. del Valle, Theoretical chemistry in solution. Some results and perspectives of the continuum methods and in particular of the polarizable continuum model, J. Mol. Struct. THEOCHEM. 234 (1991) 401–424. https://doi.org/10.1016/0166-1280(91)89026-W.
[46] A. Fortunelli, J. Tomasi, The implementation of density functional theory within the polarizable continuum model for solvation, Chem. Phys. Lett. 231 (1994) 34–39. https://doi.org/10.1016/0009-2614(94)01253-9.
[47] R.E. Grisenti, W. Schöllkopf, J.P. Toennies, G.C. Hegerfeldt, T. Köhler, M. Stoll, Determination of the Bond Length and Binding Energy of the Helium Dimer by Diffraction from a Transmission Grating, Phys. Rev. Lett. 85 (2000) 2284–2287. https://doi.org/10.1103/PhysRevLett.85.2284.
[48] M.J. Bentel, Y. Yu, L. Xu, Z. Li, B.M. Wong, Y. Men, J. Liu, Defluorination of per-and polyfluoroalkyl substances (PFASs) with hydrated electrons: structural dependence and implications to PFAS remediation and management, Environ. Sci. Technol. 53 (2019) 3718–3728.
[49] M.C. Hansen, M.H. Børresen, M. Schlabach, G. Cornelissen, Sorption of perfluorinated compounds from contaminated water to activated carbon, J. Soils Sediments. 10 (2010) 179–185.
[50] Z. Du, S. Deng, Y. Chen, B. Wang, J. Huang, Y. Wang, G. Yu, Removal of perfluorinated carboxylates from washing wastewater of perfluorooctanesulfonyl fluoride using activated carbons and resins, J. Hazard. Mater. 286 (2015) 136–143.
[51] N. Merino, Y. Qu, R.A. Deeb, E.L. Hawley, M.R. Hoffmann, S. Mahendra, Degradation and removal methods for perfluoroalkyl and polyfluoroalkyl substances in water, Environ. Eng. Sci. 33 (2016) 615–649.
[52] C. Costentin, M. Robert, J.-M. Savéant, Stepwise and concerted electron-transfer/bond breaking reactions. Solvent control of the existence of unstable π ion radicals and of the activation barriers of their heterolytic cleavage, J. Am. Chem. Soc. 126 (2004) 16834–16840.

[53] X. Li, S. Chen, X. Quan, Y. Zhang, Enhanced adsorption of PFOA and PFOS on multiwalled carbon nanotubes under electrochemical assistance, Environ. Sci. Technol. 45 (2011) 8498–8505.
[54] K.C. Westaway, Determining transition state structure using kinetic isotope effects, J. Label. Compd. Radiopharm. 50 (2007) 989–1005. https://doi.org/10.1002/jlcr.1434.
[55] Z. Song, H. Tang, N. Wang, L. Zhu, Reductive defluorination of perfluorooctanoic acid by hydrated electrons in a sulfite-mediated UV photochemical system, J. Hazard. Mater. (2013). https://doi.org/10.1016/j.jhazmat.2013.08.059.
[56] F. Rust, C.M. Stevens, Carbon kinetic isotope effect in the oxidation of methane by hydroxyl, Int. J. Chem. Kinet. 12 (1980) 371–377. https://doi.org/10.1002/kin.550120602.
[57] L.C.S. Melander, W.H. Saunders, Reaction rates of isotopic molecules, John Wiley & Sons, 1980.
[58] T.B. Hofstetter, C.M. Reddy, L.J. Heraty, M. Berg, N.C. Sturchio, Carbon and chlorine isotope effects during abiotic reductive dechlorination of polychlorinated ethanes, Environ. Sci. Technol. 41 (2007) 4662–4668.
[59] K. Li, M.I. Stefan, J.C. Crittenden, UV photolysis of trichloroethylene: Product study and kinetic modeling, Environ. Sci. Technol. 38 (2004) 6685–6693.
[60] Y.-H. Chuang, S. Chen, C.J. Chinn, W.A. Mitch, Comparing the UV/monochloramine and UV/free chlorine advanced oxidation processes (AOPs) to the UV/hydrogen peroxide AOP under scenarios relevant to potable reuse, Environ. Sci. Technol. 51 (2017) 13859–13868.
[61] T.H. Lim, S.D. Kim, Trichloroethylene degradation by photocatalysis in annular flow and annulus fluidized bed photoreactors, Chemosphere. 54 (2004) 305–312.